NERA

Network of European Research Infrastructures for Earthquake Risk Assessment and Mitigation

Report

New simulation schemes (high frequencies, moderate earthquakes, near-field)

Activity:	*Near fault ground motion*
Activity number:	*JRA3, Task 13.5*
Deliverable:	*Report and software*
Deliverable number:	*D13.3*
Responsible activity leader:	*Luis Angel Dalguer (ETHZ)*
Responsible participant:	*AMRA*
Author:	*Gaetano Festa*

Seventh Framework Programme
EC project number: 262330

Summary

During the project we developed and tested four codes for broad-band ground motion generation and source characterization. Here we present the methodologies associated with the codes, the input requirements, the outputs, the performances and the availability of the codes.
EGF_K2 combines the complexity in source kinematics with empirical Green functions, which correspond to records of small events that share the same focal mechanism as the main event. Beyond the corner frequency of the EGF the simulation is stochastic. This method can be used to simulate synthetic seismograms up to 20 Hz.
Rupture Dynamic Earthquake Scenarios are instead built on dynamic rupture properties coupled with 3D numerical Green's functions, computed by a finite difference code. Rupture is nucleated by artificially raising the initial stress in a patch above the yield strength. Then the rupture naturally evolves up to stop either at the boundary of the fault or at a physical barrier. Simulated scenarios were used to complement the GMPEs in near fault region.
KIRIA is an inversion software that generates kinematic source models by strong-motion, GPS and SAR data. It is based on a global exploration and 1D numerical Green's function. The final model is obtained by a weighted average of the ensemble models. Such a technique provides strong motion data form the retrieved source model(s) up to 1Hz.
Finally SongRMG code is used to extract one-point and two points statistics from an ensemble of source models. Specifically, the goal here is to provide kinematic models whose characteristics are compatible with rupture dynamics. They can be used as input source models for ground motion generation or to constrain the inverse problem.

Introduction and structure of the deliverable

Damage associated with moderate to large earthquakes mainly occurs in the fault vicinity and exhibits a strong spatial variability. This is the case of the 2008, M6.9 Iwate-Miyagi, Japan, earthquake, where 4g acceleration was recorded at one station located at the top of the fault, or the case of the 2009, M6.3 L'Aquila, Italy, earthquake, which produced a significant and scattered damage despite its moderate magnitude. Both aspects are currently missing in ground motion prediction equations which oversimplify the description of the rupture process and its coupling with the waves in the near-field/near-source region.

Source and propagation complexity could be nowadays tackled by broad-band ground motion simulations, that may account for the specific source geometry, a complex propagation in a tridimensional geological structure and local site effects. Such simulations can be made realistic by the impressive increase of the computational resources that allow for faster computation and a large amount of scenarios and by the increasing knowledge on the fault and medium structure, in terms of geometry and mechanical properties.

To make simulations competitive with the standard probabilistic approach for hazard assessment, a large number of scenarios are required to assess the statistical properties of the ground motion parameters in terms of mean, median and variance, as well as in terms of spatial variability.

Here we present four techniques generating broad-band strong motion data from a complex description of the fault and the structure. Depending on the method, rupture evolution is described by its kinematic or dynamic parameters. Specifically kinematic models are straightforward in the ground motion computation because they can be directly coupled with the Green's traction, these latter being computed once for a single case study, at the beginning of the computation. On the other hand, dynamic simulations include the physical properties of the rupture and may account for the causal stress release on the fault itself. To take advantage of the kinematic description of the rupture but also accounting for the physical evolution of the fracture, an effort was done in this Work Package, to investigate dynamically compatible kinematic models.

Finally, Green's functions are either numerically computed, in 1D to 3D structures, or replaced by the records of small earthquakes, that behave as Empirical Green's functions when sharing the same focal mechanism of the main event. The four techniques, hence, combine one specific source description with one specific way to compute the Green's function, to produce broad-band ground motion simulations.

The report contains the description of the four codes. For each code, after summarizing the main characteristics, we describe the methodology, the inputs, the outputs, the performances, an example and finally the software availability.

EGF_K2

Short summary

Authors: **S. Del Gaudio, M. Causse, G. Festa**
Institutions: **AMRA, ISTerre**

Code level: Research
Language: Matlab
Rupture description: Kinematic
Green's function comp. method: Empirical / Hybrid Green's Functions
Tested operating system: Linux / Windows

Software objectives

The software synthesizes a population of broadband ground-motion time histories for an hypothetical future earthquake, using the empirical Green's functions (EGFs) technique. This population maps the natural variability of the fault rupture process, and is used to assess the average and the variability of the ground motion.

The main advantage is that the small earthquake recording used as EGF naturally contains all the information about propagation and site effects, under the assumption of the linearity of the soil response. However, the EGFs must have a signal-to-noise ratio sufficiently large at low-frequency (> 2-3) to ensure accuracy of the predictions. In case of poor signal-to-noise ratio, hybrid Green's functions (HGFs), *i.e.* EGFs combined with low-frequency numerical simulations, can be used.

Methodology

Principle
The principle is to sum up EGFs (or HGFs) to simulate ground motion due to a larger earthquake, following the classical scaling law of Brune (1970). The summation algorithm results in an apparent source time function, which is then convolved with the EGF to obtain ground motion.

Source description
The summation algorithm is based on a k^{-2} kinematic source model (*e.g.* Gallovic and Brokesova, 2004). The distribution of the static slip is described in the wavenumber domain by an asymptotic k^{-2} decay beyond the corner wavenumber K/L, where L is the rupture dimension. K is an non-dimensional parameter that controls the roughness degree of slip heterogeneity. The rise time is inversely proportional to the slip wavenumber. The rupture velocity is constant. The small scale slip heterogeneities are assumed to have random rupture directions. This choice strongly reduces directivity effect at high frequency.

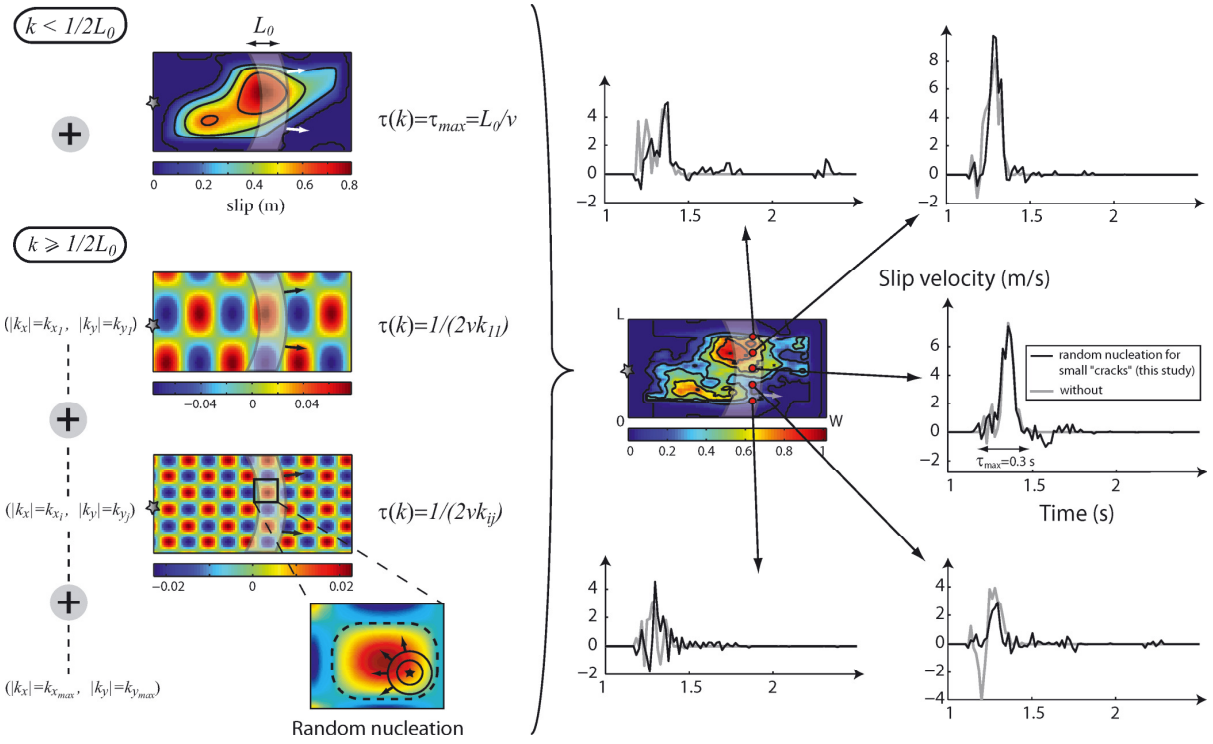

Figure 1: Representation of the rupture process, modeled as a slip pulse propagating at constant rupture velocity v. The slip distribution is split into its low and high components at frequency k = $1/2L_0$. The low wavenumber slip has a rise time equal to $\tau_{max} = L_0/v$. The high wavenumber slip is composed of a set of heterogeneities of different scales, considered as independent subevents. These subevents start slipping as the main rupture front reaches one point, randomly chosen, from which a secondary rupture front propagates (see bottom left box). The slip duration for a given subevent is proportional to its wavenumber. The figure also displays example of resulting slip velocity functions. In this example, L = 5 km, W = 2.5 km, D = 0.2 m, K = 1 and τ_{max} = 0.3 s, where L is the rupture length, W is the rupture width, K is the slip roughness parameter and τmax is the rise time.

Summation process beyond the EGF corner frequency (f_c)

Beyond f_c, the energy of the simulated event is purely stochastic because the EGF summation is incoherent. The summation algorithm is then adapted to ensure that the theoretical spectral level of the apparent source time function (*i.e.* in agreement with the kinematic source model) is obtained. Hence, the code can reasonably be used to model the source process at frequencies up to 20 Hz. Nevertheless, the user should keep in mind that the source process becomes purely stochastic beyond f_c.

Modelling ground-motion variability

The ground-motion variability is assessed by defining the source parameter uncertainties and calculating their effects on the ground-motion. The source parameters have their own assigned probability density functions. The Latin Hypercube Sampling method (McKay 1988) is next applied to select for each parameter a set n of values, chosen according to its distribution. These values are combined for obtaining a set of n samples of source parameters. Finally, the resulting parameter combinations are used to simulate a class of n response spectra, from which the median and standard deviation are estimated.

Input

EGF parameters

- Moment magnitude

- Position (epicentral distance, depth, source-receiver azimuth)

Note that the EGF focal mechanism must be in agreement with the one of the simulated event.

Source parameters
- Moment magnitude of the simulated event
- Fault plane parameterization (size, strike and dip angles)
- Rise time
- Rupture velocity, roughness parameter (non-dimensional parameter K) and position of the rupture nucleation.

Note that these parameters are not defined by assigning a single value but through probability density functions.

Output

The output of the code is a suite of accelerograms and associated response spectra, as well as the mean and standard deviation of spectral acceleration.

Performances

Computation time can vary from few seconds to few minutes depending on the number of the simulations and in particular on the fault plane discretization, which depends on the difference in moment magnitude between the target event and the EGF.

Example

As a case test, the results of the simulations for the 2009, L'Aquila earthquake, are shown. Empirical Green functions were completed at low frequency, where the signal to noise ratio is not large by 1D and 3D numerical Green's functions. Simulations were compared with real data both for near source AQ stations and far source stations. Comparison of synthetic Fourier amplitude spectra and response spectra are shown in Figure 2 for two stations, one very close to the epicenter (AQU) and the other one in far source condition (FMG).
The influence of the source parameters and their distribution on the fault plane on the ground motion was also investigated. Specifically the synthetic spectrum at high frequency well fit the real one when the rise time rapidly changes in a broad interval [0.1s – 1s], as shown in Figure 2, where synthetic spectra were obtained with constant and variable rise time respectively.
Finally when generating a large amount of synthetic spectra for the strong motion stations, changing the slip distribution at high frequency, the rupture velocity and the empirical Green function, used as a propagator, the variability of the simulated spectra can be as large as one order of magnitude. For the far source stations the mean estimate well describes the real data while real spectra at L'Aquila stations lie well below the mean value of the simulations, although they still fall within two sigma in the whole frequency range.

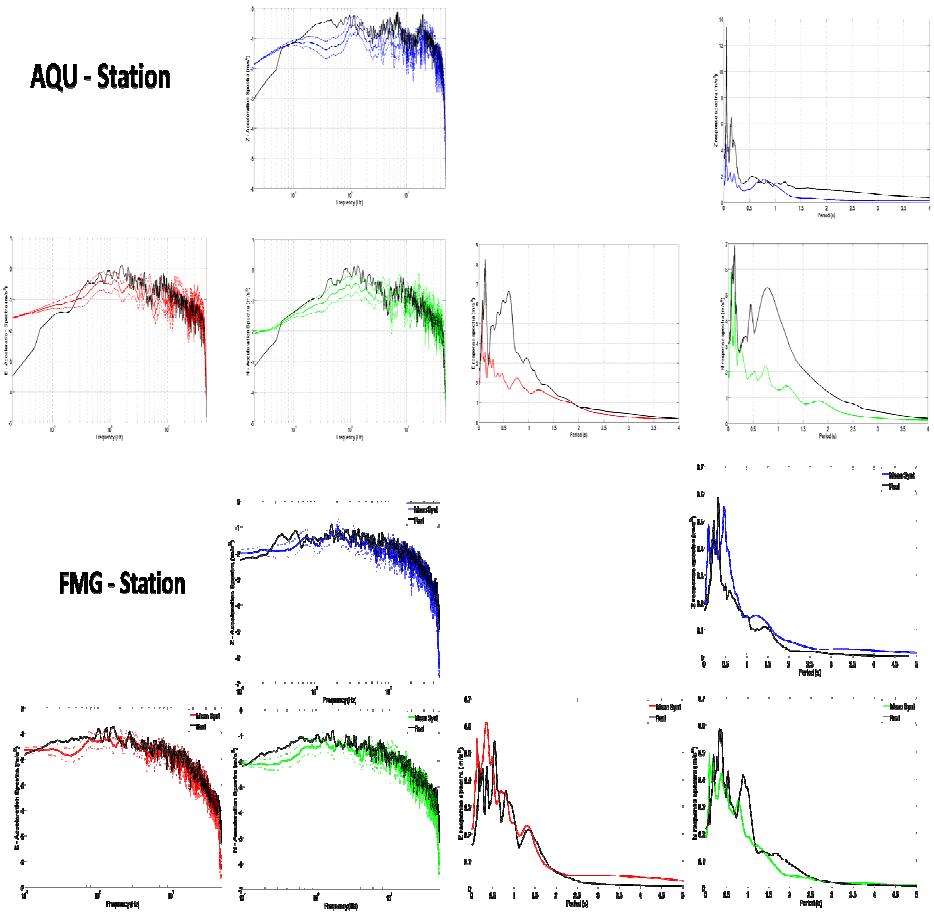

Figure 2: Simulated Fourier and response spectra for two stations compared to real data (black curve).

Related publications

M. Causse, E. Chaljub, F. Cotton, C. Cornou, P.Y. Bard (2009). New approach for coupling k-2 and empirical Green's functions: application to the blind prediction of broad-band ground motion in the Grenoble basin, *Geophys. J. Int.* 179, 1627-1644.

General references

J. Brune (1970). Tectonic stress and the spectra of seismic share waves from earthquakes, J. Geophys. Res. 75, 4997-5009.
F. Gallovic, J. Brokesova (2004). On strong ground motion synthesis with the k-2 slip distribution, J. Seism. 8, 211-224.
M.D. McKay (1988). Sensitivity and uncertainty analysis using a statistical sample of input values, in *Uncertainty Analysis*, 145-186, ed. Y. Ronen, CRC Press, Boca Raton, Florida.

Software availability

The software is available on demand to Sergio Del Gaudio (sergio.delgaudio@unina.it).

KIRIA: Kinematic Rupture Inversion Algorithm

Short summary

Authors:	**A.Cirella, A. Piatanesi, P. Spudich**
Institutions:	**INGV, USGS**
Code level:	Research
Language:	Fortran 77
Rupture description:	Kinematic
Green's function comp. method:	Discrete wave number - Finite Element integration technique
Tested operating system:	Linux, Mac OSX

Software objectives

KIRIA is a code to image the earthquake source process on a finite fault, from inversion of seismological and geodetic data.

Methodology

KIRIA is a two-stage nonlinear technique to retrieve the rupture history of an earthquake on a finite fault, from the inversion of strong motions records and geodetic data.
To account for the rupture complexity, the fault parameters are the spatially variable peak slip velocity, slip direction, rupture time and rise time. The extended fault plane is divided into subfaults. The unknown parameters are given at the nodes of the subfaults, whereas the parameters within a subfault are allowed to vary through a bilinear interpolation of the nodal values (Piatanesi et al., 2007). The forward modeling is performed with a discrete wavenumber technique, whose Green's functions include the complete response of a vertically varying Earth structure. During the first stage, an algorithm based on the heat-bath simulated annealing generates an ensemble of models that efficiently sample the good data-fitting regions of parameter space. In the second stage (appraisal), the algorithm performs a statistical analysis of the model ensemble and computes a weighted mean model and its standard deviation. This technique, rather than simply looking at the best model, extracts the most stable features of the earthquake rupture that are consistent with the data and gives an estimate of the variability of each model parameter. We adopt a single window approach where each point on the fault can slip only once following a prescribed functional form of the source time function (STF). Our technique has been implemented to allow for the choice of different slip velocity STFs (Cirella, 2008).
To obtain ground displacements we use the representation theorem of Spudich (1980) to calculate ground motions:

$$\overline{u}_k(\mathbf{x},\omega) = \int_S \overline{\mathbf{s}}(\xi,\omega) \bullet \overline{\mathbf{T}}_k(\xi,\omega;\mathbf{x}) d\xi$$

where $\mathbf{x}$ is the position of the observer, $\boldsymbol{\xi}$ is the local coordinate system on the fault plane S, k denotes the x, y or z direction, $\overline{u}_k(\mathbf{x},\omega)$ is the Fourier transform of the k-component of displacement at observer location $\mathbf{x}$ and angular frequency ω, $\overline{\mathbf{s}}(\xi,\omega)$ is the Fourier transform of the slip vector at point $\boldsymbol{\xi}$ on the fault and $\overline{\mathbf{T}}_k(\xi,\omega;\mathbf{x})$ is the Fourier transform of the traction vector at a point $\boldsymbol{\xi}$ on the fault caused by a point impulsive force in the k-direction at observer location $\mathbf{x}$. This form of the representation theorem uses Green's function reciprocity.

We calculate the traction Green's functions on the fault plane using a discrete wavenumber integration technique that allows for the complete response in a vertically varying medium (Spudich and Xu, 2003). The ground displacement (or velocity) at an observer non-linearly depends on the kinematic rupture history. Instead of linearizing the problem and applying a linear inverse theory, we use a global optimization method to search for the source parameters. In particular we implemented a special flavor of the simulated annealing technique, called the "heat-bath" algorithm, which is very efficient for exploring high dimensional model spaces (Sen and Stoffa, 1995). The algorithm works by perturbing the model parameters one by one; for this reason, synthetic seismograms from only those subfaults sharing the current nodal parameter need to be updated at each perturbation, thus reducing the computational time.
Since the forward modeling is relatively fast for computing waveform spectra, recorded and synthetic seismograms are compared in the frequency domain, using both real and imaginary parts of the signal's spectra. A main point in inverse problems is the choice of a suitable cost function to represent the goodness of a model. For waveform spectra, we use an objective function that is a hybrid representation between L1 and L2 norm (Piatanesi et al., 2007). This cost function takes information from both the shape and the amplitude of a waveform and it turns out that it is more robust than standard least squares. The cost function, related to near-field GPS and DInSAR measurements, is a sum-squared of the residuals between synthetic and observed static displacements (see Cirella et al., 2008, for further details), normalized to the observed data.
The algorithm consists of two stages. During the first stage, the heat-bath simulated annealing algorithm extensively explores the model space to generate an ensemble of models that efficiently sample the good data-fitting regions. The simulated annealing technique follows the analogy with annealing in thermodynamics, consisting in slowly cooling the system toward the minimum energy state. Ideally, large sampling of the model space is achieved by starting the algorithm at relatively high temperature and slowly cooling the system towards the critical temperature, at which the system is expected to reach the minimum energy state (i.e. minimum of the cost function). Since we deal with a very large dimension of the model space (typically more than 200 parameters are inverted) a true simulated annealing cannot be realized, because the ideal cooling would require an excessive CPU time and a simulated quenching is performed instead. In the latter case, the cooling is faster than in the ideal annealing and the sampling of the model space may be slightly dependent on the choice of the starting model; for this reason the algorithm is conceived to perform several restarts with different random trial models, in order to make the model ensemble independent from a particular choice of the initial model. During the search, all models that are visited and the corresponding values of the cost function are saved to build the model ensemble. The second stage of the algorithm is the ensemble inference. The underlying idea is that basing inferences on an ensemble of potential solutions convey more information than considering just the best. In fact, limiting the analysis to the features present only in the best fitting model is often insufficient because of non-uniqueness in the problem and noise in the data. We compute an averaged model parameter and the associated standard deviation by weighting all models of the ensemble by the inverse of their cost function values. Let m_{ij} be the i-th parameter of the j-th model belonging to the ensemble and E_j the cost function corresponding to the model $\mathbf{m}_j$. The averaged model parameter $\langle m_i \rangle$ and the corresponding standard deviation $\langle \sigma_i \rangle$ can be obtained as the weighted mean and standard deviation among all models.
The estimates $\langle m_i \rangle$ and $\langle \sigma_i \rangle$ represent the ensemble properties and are the actual solution of our nonlinear inverse problem. The novelty of this approach is the use of a very large model ensemble, built up by means of multiple restarts of the annealing algorithm, to take advantage from the whole search process instead of looking only at the best model.
The maximum frequency that can be reasonably simulated with the code is 0.8-1.0 Hz.

Input

The inputs required by the code are:

- Strong Motion (processed in the frequency band of interest), GPS and DInSAR data;
- Crustal structure in terms of 1D velocity profiles for all recording stations;
- Focal Mechanism;
- Fault Geometry;

We invert simultaneously for all the parameters at nodal points equally spaced along strike and dip directions. During the inversion, we provide a given range of variability for each model parameter.

Output

The main output of the code is the complete kinematic description of the rupture process in terms of peak slip velocity, slip angle, rise time and rupture time distributions on the fault plane. For each inverted model parameter the technique yields the corresponding best, average distribution and the associated standard deviation.

Example

As an example we shows here the rupture process of the 2009 M_W=6.1 L'Aquila (central Italy) earthquake retrieved from non linear inversion of strong motion, GPS and DInSAR data.

Data

We have selected 13 three-component digital accelerometers of the RAN Network (http://itaca.mi.ingv.it/ItacaNet) and the AQU (MedNet) accelerogram (see Figure 3). They were integrated to obtain ground velocity time histories and band-pass filtered between 0.02 and 0.5 Hz with a two-pole and two-pass Butterworth filter. We have considered 36 three-component GPS displacements inferred from measurements at the closest receivers (see Figure 3). We have inverted the DInSAR interferograms shown in Figure 4 (obtained from ENVISAT and ALOS SAR data), which represent the deformation along the LoS of the satellites. The looking angles of the two satellites are 23° and 36° for ENVISAT and ALOS respectively, and we compute the synthetic deformation along the LoS direction (Cirella et al., 2012).

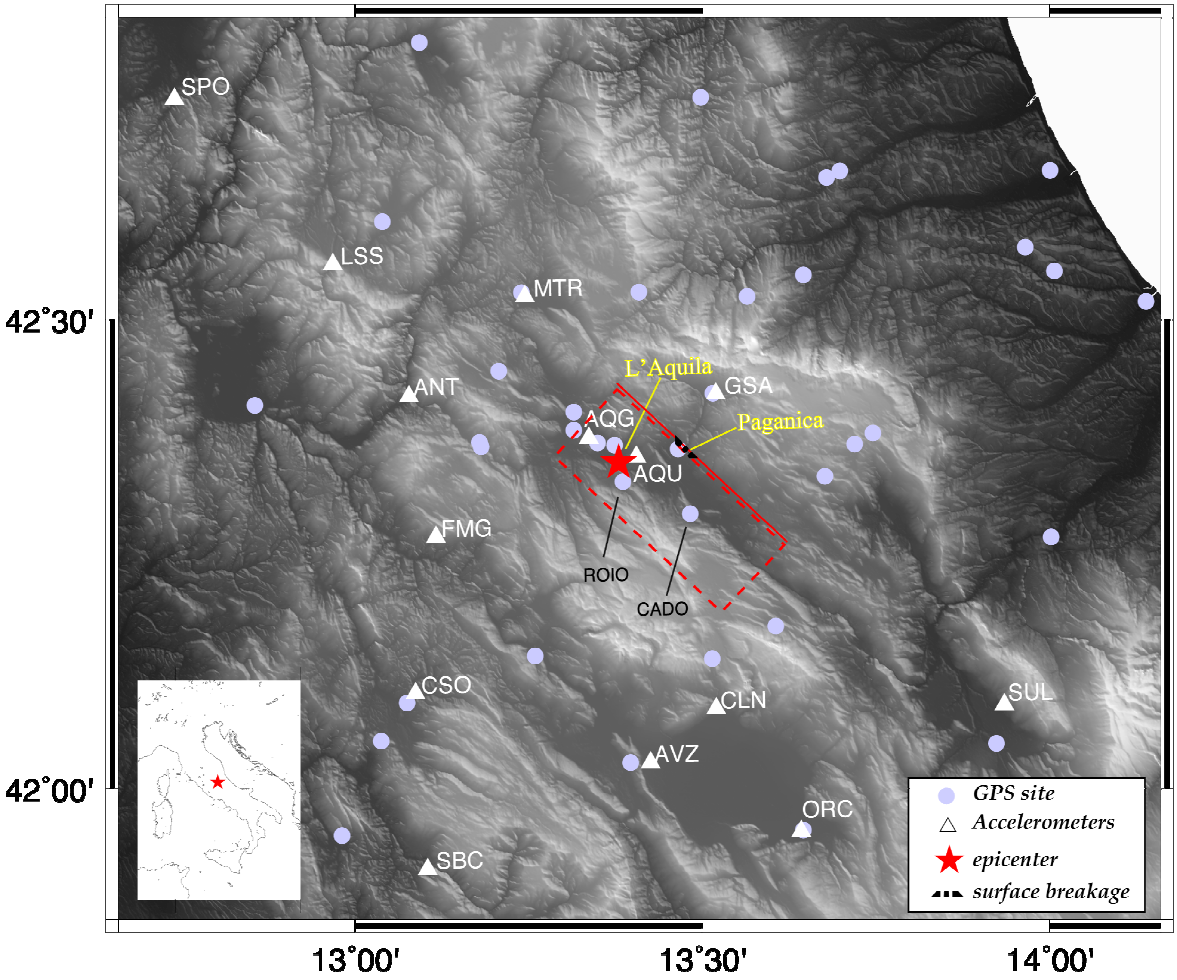

Figure 3. Map of the fault geometry of the 2009 L'Aquila earthquake. The red box represents the surface projection of the fault plane adopted in this study. White triangles represent the selected strong motions stations. Violet dots represent the GPS sites, The red star indicates the epicenter. In yellow are displayed the location of the L'Aquila town and Paganica village.

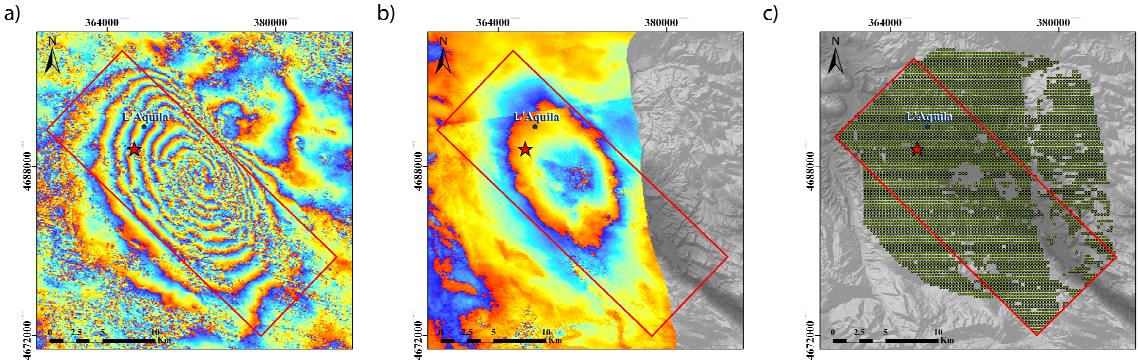

Figure 4. a) Envisat wrapped interferogram; b) ALOS wrapped interferogram; c) Green color shows the 4599 resampled pixels (size 300m), from both interferograms, selected in this study. The red rectangle represents the surface projection of the fault plane fixed for this study, while the red star represent the epicenter.

Crustal Structure

For computing the Green's functions, we have assumed for all recording stations (except for AQU and AQG) the 1D velocity model proposed by Herrmann et al. (2011), and

calibrated during the sequence through the analysis of surface wave dispersion. For AQU and AQG seismic stations we have adopted a 1-D velocity model specific for these receivers obtained by the analysis of receiver functions (Bianchi et al. 2010).

Fault model and Parametrization

The adopted fault plane, striking N133°E and dipping 54° to the SW (Cirella et al. 2009), is 28 km long and 17.5 km wide with the shallow top border located at 0.5 km depth just below the surface breakage observed along the Paganica. We assume the INGV hypocenter (Chiarabba et al. 2009).

We invert simultaneously for all the parameters at nodal points equally spaced (3.5 km) along strike and dip directions. During the inversion, we fix a given range of variability for each model parameter. In particular, in this study we adopt the following variability intervals: peak slip velocity values can range between 0 and 3.5 m/s at 0.25 m/s interval; the rise time between 0.75 and 3 sec at 0.25 sec interval and the rake angle from 230° to 310° in steps of 10°. The rupture time at each grid node is constrained by the arrival time from the hypocenter of a rupture front having a speed comprised between 1.4 and 4 km/s.

Results

The inferred average rupture model is shown in Figure 5a. The three panels on the left display the computed slip distribution, the inverted rise time and peak slip velocity distributions, respectively. The black arrows on the top-left panel show the slip direction, the white contour lines display the rupture time distribution on the fault plane. The three panels on the right (Figure 5b) display the distribution on the fault plane of the coefficient of variation for the rupture times (top panel), the rise time (middle panel) and the peak slip velocity (bottom panel). In each of these three panels the white contour lines display the spatial distribution of the associated model parameter.

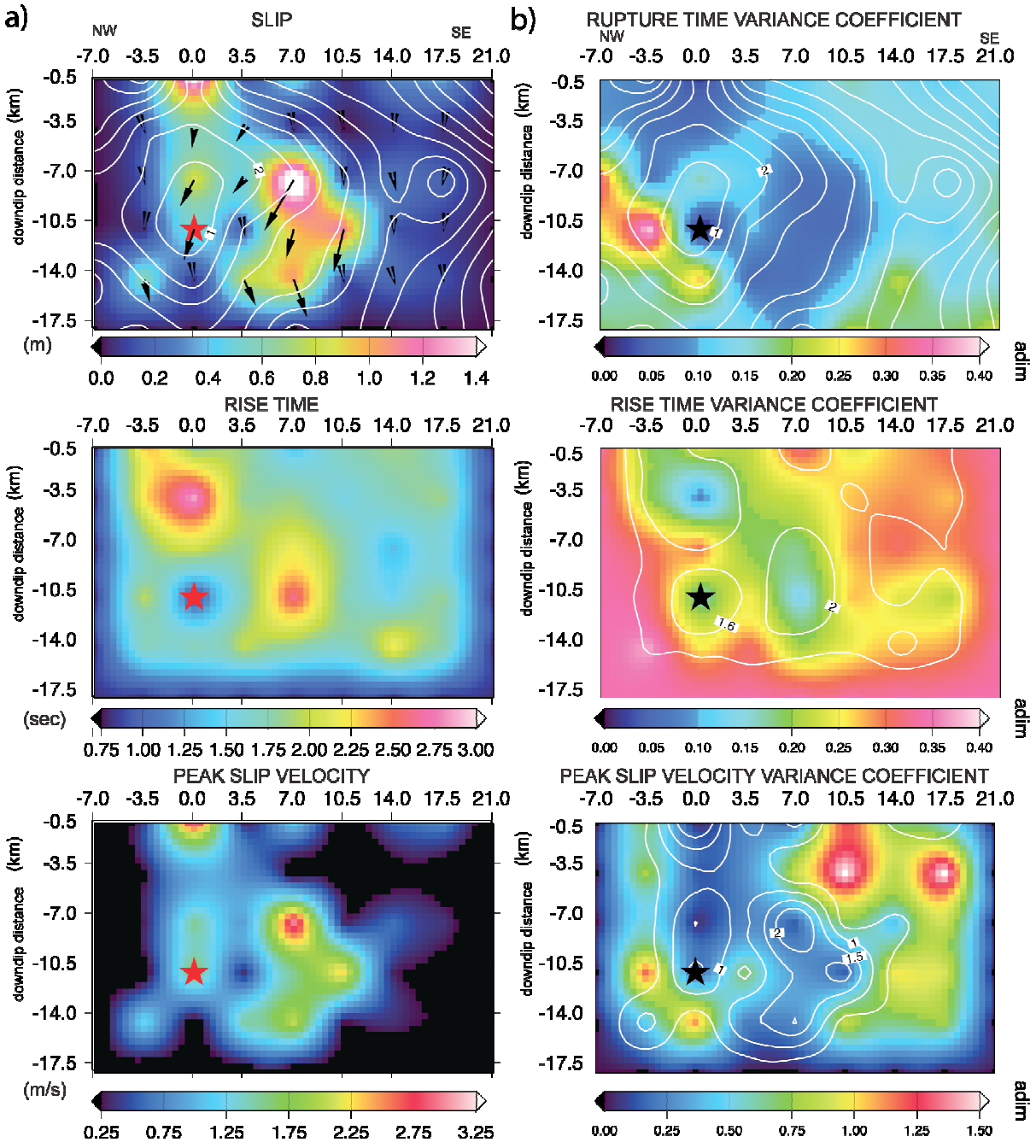

Figure 5. a) Inverted rupture model (average model from ensemble inference) of the 2009 L'Aquila earthquake. Upper, middle and bottom panels show total slip, rise time and peak slip velocity distributions, respectively. The rupture time is shown by contour lines in white color at 1s intervals; the black arrows displayed in top panel represent the slip vector; b) Coefficient of variation (CV). Top, middle and bottom panels display the rupture times, the rise time and the peak slip velocity spatial distributions of the CV, respectively. White contour lines in each panel display the spatial distribution of the associated model parameter.

Related publications

Cirella A., Piatanesi A., Tinti E. Chini M. and M. Cocco (2012), "Complexity of the rupture process during the 2009 L'Aquila, Italy, earthquake", Geophysical Journal International.190, 607-621, doi:10.1111/j.1365-246X.2012.05505.x.

Cultrera G., Ameri G., Saraò A., Cirella A. and A. Emolo (2012) "Ground-motion

simulations within ShakeMap methodology: application to the 2008 Iwate-Miyagi Nairiku (Japan) and 1980 Irpinia (Italy) earthquakes" accepted 2012 November 15 for publication in Geophysical Journal International.
Avallone, A, M. Marzario, A. Cirella, A. Piatanesi, A. Rovelli, C. Di Alessandro, E. D'Anastasio, N. D'Agostino, R. Giuliani, M. Mattone (2011), "Very high rate (10 Hz) GPS seismology for moderate-magnitude earthquakes: The case of the M(w) 6.3 L'Aquila (central Italy) event" Journal of Geophysical Research - Solid Earth, Volume: 116, B02305, doi:10.1029/2010JB007834.
Scognamiglio L. ,Tinti E., Michelini A., Dreger D., Cirella A., Cocco M., Mazza S., and Piatanesi A. (2010), "Fast Determination of Moment Tensors and Rupture History: Application to the April 6th 2009, L'Aquila Earthquake", Seismological Research Letters, Volume 81, number 6, Novembre/December 2010, doi: 10.1785/gssrl.81.6.892.
Cirella, A., A. Piatanesi, M. Cocco, E. Tinti, L. Scognamiglio, A. Michelini, A. Lomax, and E. Boschi (2009), "Rupture history of the 2009 L'Aquila earthquake from non-linear joint inversion of strong motion and GPS data", Geophys. Res. Lett. 36, L19304, doi:10.1029/2009GL039795.
Cirella A., Piatanesi A., Tinti E. and M. Cocco (2008). "Rupture process of the 2007 Niigata-ken Chuetsu-oki earthquake by non-linear joint inversion of Strong Motion and GPS data" Geophys. Res. Lett., 35, L16306, doi:10.1029/2008GL034756.
Cirella Antonella, "Joint Inversion of GPS and Strong Motion Data for Earthquake Rupture Models", 2008, tesi di dottorato, URI: http://hdl.handle.net/2122/5657, appears in Collections: Theses, 04.06.03. Earthquake source and dynamics.
Piatanesi A., A. Cirella, P. Spudich and M. Cocco (2007), "A global search inversion for earthquake rupture history: Application to the 2000 western Tottori, Japan earthquake", J. Geophys. Res., 112(B7), B07314, doi:10.1029/2006JB004821.

General references

Bianchi, I., C. Chiarabba, and N. Piana Agostinetti, (2010), Control of the 2009 L'Aquila earthquake, central Italy, by a high-velocity structure: A receiver function study*, J. Geophys. Res*., 115, B12326, doi:10.1029/2009JB007087.
Chiarabba, C., A. Amato, M. Anselmi, P. Baccheschi, I. Bianchi, M. Cattaneo, G. Cecere, L. Chiaraluce, M. G. Ciaccio, P. De Gori, G. De Luca, M. Di Bona, R. Di Stefano, L. Faenza, A. Govoni, L. Improta, F. P. Lucente, A. Marchetti, L. Margheriti, F. Mele, A. Michelini, G. Monachesi, M. Moretti, M. Pastori, N. Piana Agostinetti, D. Piccinini, P. Roselli, D. Seccia, and L. Valoroso, (2009), The 2009 L' Aquila (central Italy) Mw 6.3 earthquake: Main shock and aftershocks, *Geophys. Res. Lett*., 36, L18308, doi:10.1029/2009GL039627.
Herrmann, R.B. Malagnini, L., and I. Munafo, (2011), Regional Moment Tensors of the 2009 L'Aquila Earthquake Sequence, Bull. Seismol. Soc. Am., 101, No. 3, pp. 975-993.
Sen, M. and Stoffa P.L. (1995), Global Optimization Methods in Geophysical Inversion, Adv. Explor. Geophys., vol. 4, Elsevier Sci., New York.
Spudich, P. (1980), The DeHoop-Knopoff representation theorem as a linear inversion problem, Geophys. Res. Lett., 9, 717-720.
Spudich, P. and L. Xu, (2003), Software for calculating earthquake ground motions from finite faults in vertically varying media, in International Handbook of Earthquake and Engineering Seismology, Academic Press.

Software availability

KIRIA is available on demand (antonella.cirella@ingv.it, alessio.piatanesi@ingv.it); to date there isn't a user manual for this software.

Rupture Dynamic Earthquake Scenarios

Short summary

Author(s):	**L. Dalguer**
Institution(s):	**ETH Zurich**

Code level:	Research
Language:	Matlab
Rupture description:	Dynamic rupture
Green's function comp. method:	N/A
Tested operating system:	Linux

Objectives

We have developed dynamic rupture earthquake scenarios (Dalguer and Mai, 2011, 2012) with the objective to investigate ground motion variability dominated by the source and the development of synthetic ground motion prediction equations (GMPE). This database has been verified against empirical GMPE (Baumann and Dalguer, 2013). We describe here the methodology to build dynamic rupture models and provide matlab scripts to read the earthquake database. Data consist of final slip, peak slip rate, rupture time of 360 dynamic rupture models in the range of Mw ~5.5-7.0 and resulted near-field synthetic seismograms on a dense near-source receiver grid. The models are for three classes of faulting (thrust, normal and strike slip) for buried and surface-rupturing earthquakes. Stress and frictional strength consider two extreme cases of normal stress, 1) depth-dependent, and 2) depth-independent. There are 30 models for each subcase.
Calculations were developed using the Support Operator Rupture Dynamics code (SORD). The SORD code (Ely et al., 2008, 2009) is based on a generalized Finite Difference scheme that can utilize meshes of arbitrary structure and incorporate irregular geometry, with the capability to model general fault geometry and topography. The code is freely available in the internet (http://gely.github.io/coseis/www/index.html)

Dynamic rupture model parameterization methodology

Assuming that shear failure on pre-existing faults of shallow earthquakes is governed by Coulomb friction, the mode of faulting and the loading history in compressional and extensional tectonic regimes play an important role in determining the initial stress and the absolute value of frictional strength on the fault (e.g. Sibson, 1991).

Normal Stress Depth Dependent Model.
Stress parameterization follows the methodology proposed by Dalguer and Mai (2008) to estimate the strength and initial stress on the fault prior to rupture. Their approach combines stochastic initial stress fields with a realistic fault-loading environment in which the tectonic loading regime (compressional or extensional) and the gravitational loading determine the absolute value of fault frictional resistance and initial stress. The procedure is as follows:
1) Assume that far-field stress is initially equal to the confining pressure, which is equivalent to the gravitational load

$$\sigma_1=\sigma_2=\sigma_3= \rho g h$$

where σ_1, σ_2 and σ_3, are respectively the principal stresses, ρ the density, g the acceleration of gravity and h the depth.

2) Loading of principal stresses. Increase σ_1 for thrust or strike-slip faulting; or decrease σ_3 for normal faulting events; this represents a "loading" or stress-increasing mechanism for thrust/strike-slip events, and an "unloading" or stress-reduction mechanism for normal faults.

$$\sigma_1 = \rho g h + \Delta\sigma_{load} \qquad \text{loading}$$
$$\sigma_3 = \rho g h + \Delta\sigma_{load} \qquad \text{unloading}$$

where $\Delta\sigma_{load}$ is the stress increment/decrement to load/unload the system.

3) Estimate the normal stress acting on a specific fault plane from the loaded/unloaded principal stresses.

4) Estimate the frictional strength (assuming Coulomb friction), based on the cohesion stress, the pore pressure, the effective normal stress, and the friction coefficient that depends on slip (slip weakening model) in the form given by Andrews (1976)-

5) Estimate initial shear stress on the fault as

$$\tau_0 = \tau_{st} + \Delta\tau_{ld}$$

where τ_{st} is a heterogeneous stress field (Ripperger et al., 2007, 2008) generated as a spatial random field that represents the remaining stress from the history of previous events. This stochastic stress is first tapered in an arbitrary non-depth dependent frictional strength profile such that its maximum (τ_{max}) is close to the static failure stress (τ_s) and its minimum (τ_{min}) is the final stress from the last past earthquake characterized with the dynamic overshoot ($k_{osd} > 1$) or undershoot ($k_{osd} < 1$) coefficient.

$$\tau_{\max} = \tau_s; \qquad \tau_{\min} = \tau_s - (\tau_s - \tau_d)k_{osd}$$

Finally, the τ_{st} is again tapered to the depth dependent frictional strength profile calculated in Step 4, but keeping the same ratio $(\tau_0 - \tau_d)/(\tau_s - \tau_d)$, where τ_s and τ_d are respectively the static and dynamic frictional strength. $\Delta\tau_{ld}$ in Equation 6 is a small stress increment for additional loading in the nucleation zone in order to initiate rupture instability (Ripperger et al 2007, 2008).

6) Determine the size of the nucleation zone, a circular patch with radius L_c, half of the critical length of an equivalent uniform fault with initial stress and frictional strength corresponding to the average over the fault. L_c has the form (e.g, Day et al, 2005):

$$L_c = \frac{\mu d_0 (\tau_{bav})}{\pi (\Delta\tau_{av})^2}$$

where μ is the shear modulus and τ_{bav} and $\Delta\tau_{av}$ are respectively the average breakdown strength drop and average stress drop. Depending on the stress parameterization, L_c may take on large values. Because large nucleation regions would influence the dynamic rupture properties over a large fault area, it is necessary to choose L_c as small as possible. Our numerical experiment shows that with L_c = 2.0 km is often enough to trigger rupture, so we assumed a maximum L_c of 2.0 km. The center of the nucleation zone is given stochastically, defined as the point in which the initial stress is equal to the yielding stress, as defined in step (5).

7) Shallow part, brittle crust and ductile zone. As shown in Figure 6, our parameterization considers stable zone (shallow part), brittle crust (seismogenic zone)

and ductile zone (deepest layer). The normal stress depth dependent parameterization produces a weak zone in the shallow depth unable to maintain large shear stress. If this shallow depth is not parameterized in an appropriate way, early and unrealistic rupture process may take place in this zone. In addition, some studies (e.g. Brune and Anooshehpoor, 1998) suggest that rupture at this weak shallow zone should operate in a distinctive manner from the rest of the fault, such as strength hardening due to the formation of incompetent fault gouge, cracking (e.g. Marone, 1998; Marone and Scholz, 1988), or due to the presence of thick surface deposits of sediments, fissured rocks and other forms of off-fault zone damage. The main feature of this shallow depth zone is that it operates during rupture with an enhanced energy absorption mechanism. We define the first 2 km depth as a weak shallow zone, which obeys to strength hardening during frictional sliding. To model this frictional behavior, we assume negative stress drop and large critical slip distance in this zone, defined as the stable uppermost layer (Figure 6). The seismogenic zone, below the stable zone, represents the brittle crust of the Earth. We model it as an 18 km thick layer. Below this seismogenic layer, we considered a ductile zone, characterized by large critical slip distance (Figure 6). Rupture may propagate dynamically into the weak shallow layer or into the deep ductile zone, but they cannot nucleate in these regions. Once the dynamic rupture has entered these zones, it is likely to terminate soon as the energy-absorption at the crack tip exceeds the energy supplied by the propagating crack.

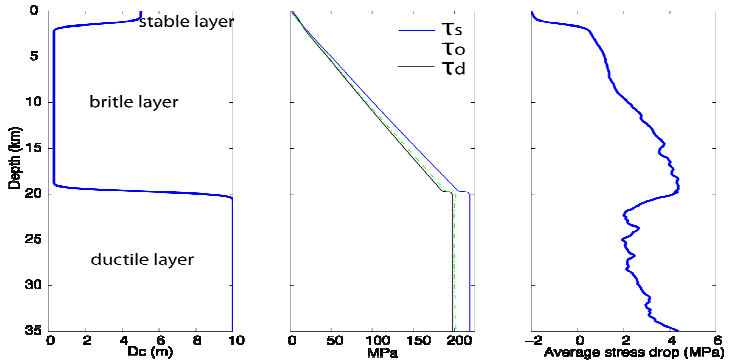

Figure 6. An example of depth variation of frictional parameters averaged along the strike of the fault, adopted in the dynamic rupture models. Left figure shows critical slip distance. Center shows the static frictional strength (τ_s), initial stress (τ_0) and dynamic frictional strength (τ_d). Right figure shows the stress drop.

Normal Stress Non-depth Dependent Model

The stress parameterization for this case follows the same procedure as described above, with the difference that the normal stress acting on the fault is constant over the fault.

Input Database

The data are located in the main subdirectories:

/ non_depth_dependent_big/ for buried fault with no depth dependent normal stress

/depth_dependent_big/ for buried fault with depth dependent normal stress

/ free_surface_non_depth_dependent_big/ for surface rupturing faults with non depth dependent normal stress

/ free_surface_depth_dependent_big/ for surface rupturing faults with depth dependent normal stress

The results of the simulations of each directory are located in the subdirectory

/s#mechanism/out/; where # is the model number (max. 30), "mechanism" is normal, reserve or strike slip. For example: /s20normal/ correspond to the normal fault model Nr 20

Dynamic rupture solutions (final slip, peak slip rate and rupture time)
They are in the subdirectory /out/ of each model. File "ss" for final slip, "trup" for rupture time, and "psv" for peak slip rate. They are binary files with little-endian format. Each file contents the information of each node on the fault, so it is a matrix of nx*ny, where nx is the number of nodes along strike and ny is the number of nodes along dip with grid size of 100m.
For reverse fault: nx=301; ny=211
Strike slip fault: nx=361; ny=181
Normal faults: nx=301; ny=211
To read them you can use the mat lab script "read_dynaf.m"

Macro Source parameters and 168 stations location data.
They are in ASCII format, located respectively for each models in:
/*/stations_fault_distance/s#mechanism.stations.dat
Where * is the main subdirectory (see above); # is the model number (max. 30), "mechanism" is normal, reserve or strike.
For example:
/depth_dependent_big/stations_fault_distance/s1normal.stations.dat corresponds to buried fault with, depth dependent normal stress, of a normal fault, model number 1.
The ASCII data is as follows:

```
% Source and stations data for PRP-Project (buried fault, depth dependent)
% Earthquake model = s1normal
% hypocenter (km) (x,y,z) =   -10.000000      4.750000     13.227241
% Moment magnitude (Mw) =   6.53
% Seismic moment (1e19 New-m) =   0.77
% Average slip (m) =   0.62
% Maximum slip (m) =   1.37
% Average slip rate (m/s) =   0.75
% Maximum slip rate (m/s) =   2.28
% Rupture area (km2) =   364.100000
% Average rupture speed (km/s) =   1.90
% Average stress drop (MPa) =     1.716544
% Max stress drop (MPa) =    10.617145
% Min stress drop (MPa) =   -10.514810
% 1st column = station number
% 2nd column = Along strike distance in km
% 3rd column = Fault normal distance in km
% 4th column = Joyner-Boore Distance (DistanceJB) in km
% 5th column = Shortest distance to the Rupture Surface (DistanceRup) in km
% 6th column = shortest horizontal distance to the line defined by extending the Fault Trace (DistanceX)
% 7th column = Side of the fault (0=footwall, 1=hanging wall)
%
=================================================================
   1   15.000000    0.300000     4.701064     8.708182     1.750000      1
   2   14.800000    0.600000     4.382921     8.561916     2.050000      1
   3   14.500000    0.800000     4.024922     8.362439     2.250000      1
…..
```

To visualize the station locations, use the mat lab script "MapStationsFault.m". An example of it is shown in Figure 7 where shows station distribution for the "s1normal"

(buried) rupture models with depth dependent normal stress.

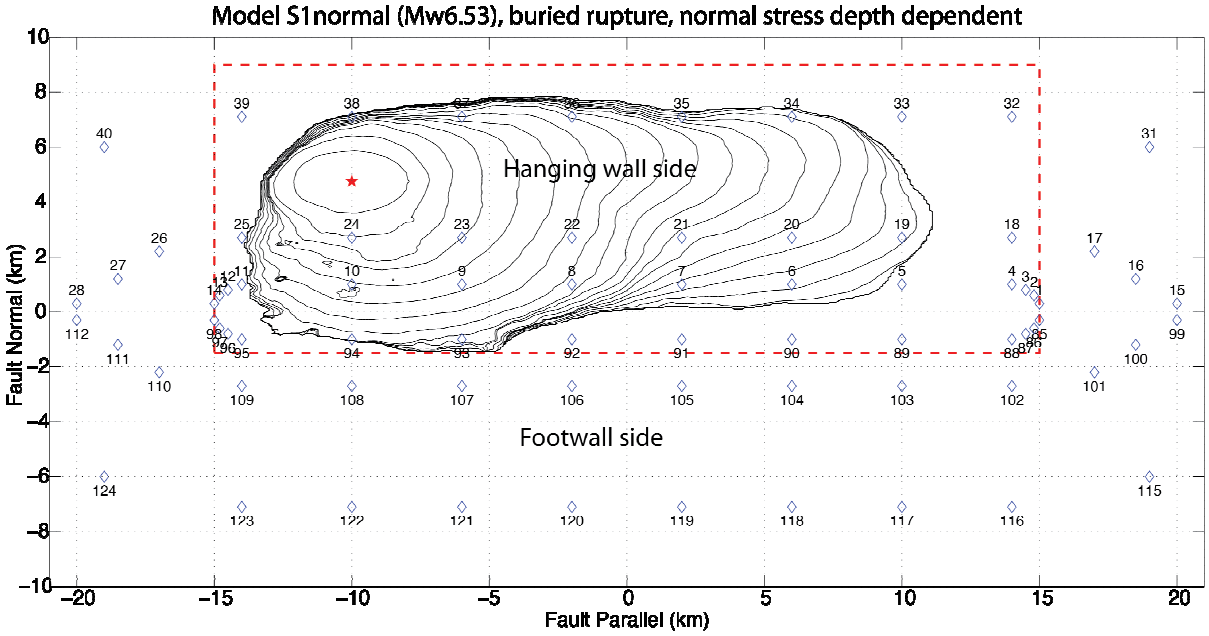

Figure 7. Close up of station location around the fault and contour rupture time of the buried fault rupture of model *s1normal*, with depth dependent normal stress. The dotted red line is the vertical projection of maximum allowed fault rupture plane. Red star denotes epicenter location.

Velocity ground motion data

They are binary little endian files. These synthetic ground motions were generated directly from the dynamic rupture simulations. The reference Swave velocity can be considered as 2500m/s. The data is located in the subdirectpry "out"

The number of stations for the hanging wall and footwall is 84, with a total of 168 stations (see figures 7 and 8 for location of them around the fault). This number of stations for each side of the fault is true for a surface-rupturing model. However, for a buried rupture model it depends of how rupture has extended on the allowed fault plane rupture.

To read this data use the matlab script "readVGMf.m"

MATLAB SCRIPTS to read data

There are different Matlab scripts. Here I describe the most important, they are self-explanatory

Matlab scripts have to be run from the main directory /ModelsDyna/

- read_dynaf.m: function to read dynamic rupture solutions on the fault (final slip, rupture time and peak slip rate). Other source parameters, such as stress drop, rupture speed you can also get after reading the matlab script.
- MapStationsFault.m: Function to have a map view of the stations location and rupture projection of the free-surface.
- readVGMf.m: Function to read three component of the Velocity wave forms.
- DynaGMestimate.m: Function to calculate 3 component of acceleration, velocity and displacement ground motion of each station. It give you also results including site amplification correction for Vs30<=1500m/s.
- DynaSA_GMPE.m: Function to calculate 3 component of acceleration, velocity and displacement ground motion of each station. In addition, it compares Spectral Acceleration with GMPE.
- DynaPgvPgaSaGMPE.m: Function to calculate PGV, PGA and PSA at period T for all stations (168) and compare with GMPEs from Akkar and Bommer (2010) denoted as AK10 and Boore and Atkinson (2008) denoted as BA08. The synthetic ground motion

data is for a reference S wave velocity of 2500m/s. For vs30 <= 1500 m/s it is estimated a Site-amplification corrections using the period dependent amplification coefficient of Borcherdt (1994, 2002).

Example

Figure 8 shows an example of the PGA and PGV compared with the GMPES for Vs30=1500m/s.

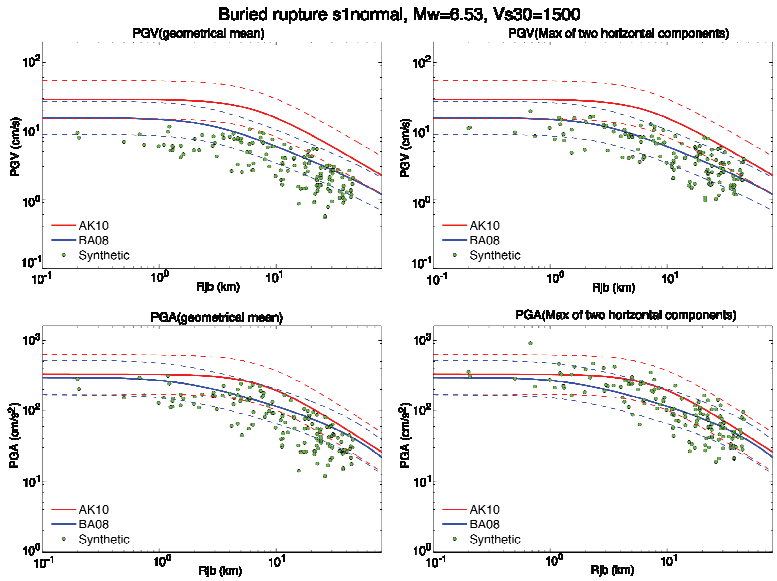

Figure 8. Horizontal PGV (top) and PGA (bottom) of buried rupture model "s1normal", depth dependent normal tress, compared with GMPE from AK10 (Akkar and Bommer, 2010) and BA08 (Boore and Atkinson, 2008) for Vs30=1500m/s. Peak values of synthetic wave forms are calculated in two ways: geometrical means (left) and maximum of two horizontal components (right)

Dynamic rupture solutions of "s1normal" and "s16normal" models

Figure 9, for s1normal dynamic rupture solution, shows slip, peak slip rate, rupture time and stress drop distribution.

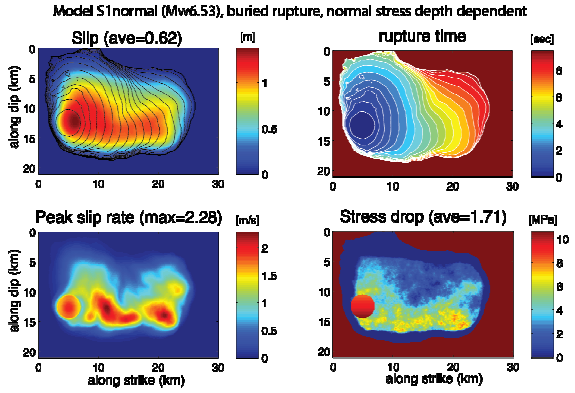

Figure 9. Dynamic rupture solutions for the buried rupture model "s1normal", depth dependent normal tress. Top left shows slip distribution (contour line is the rupture time each 0.5 sec); top right is image map and contour line of rupture time; bottom left is peak slip rate; and bottom right is the stress drop distribution.

Related publications

Baumann C. and L.A. Dalguer (2013), Evaluating the Compatibility of Dynamic-Rupture Based Synthetic Ground Motion with Empirical GMPE. Bull. Seismol. Soc. Am. In review
Dalguer L.A. and P. M. Mai (2011), Near- Source Ground Motion Variability from M~6.5 Dynamic Rupture Simulations. 4th IASPEI / IAEE International Symposium: Effects of Surface Geology on Seismic Motion, In CD. August 23–26, 2011, University of California Santa Barbara, CA, USA.
Dalguer, L.A. and P.M. Mai (2012), Prediction of near-source ground motion exceeding 1g at low frequencies (<2Hz) from Mw~6.5 deterministic physics-based dynamic rupture simulations, Proceedings of the 15th World Conference on Earthquake Engineering (15WCEE), Lisbon, Portugal, September 24-28, 2012.

Database availability

The database of the 360 dynamic rupture models is available through the implementation report (Deliverable 13.5). But it can also be download from http://www.seg2.ethz.ch/dalguer/download/DynaModels360.html or ask directly to Dr. Luis A. Dalguer (dalguer@sed.ethz.ch)

General references

Akkar, S. and J. J. Bommer (2010). Empirical equations for the prediction of PGA, PGV, and spectral accelerations in Europe, the Mediterranean region, and the Middle East, Seismological Research Letters, 81(2) 195-206.
Boore, D. M., and G. M. Atkinson (2008). Ground-motion prediction equations for the average horizontal component of PGA, PGV, and 5%-damped PSA at spectral periods between 0.01 s and 10.0 s, Earthquake Spectra 24, 99–138
Dalguer, L.A. and M. Mai (2008), Implications of Style-of-Faulting and Loading Characteristics on the Dynamic Rupture Process, Eos Trans. AGU, 89(53), Fall Meet. Suppl., Abstract S51D-1798.
Day, S. M., L. A. Dalguer, N. Lapusta, and Y. Liu (2005), Comparison of finite difference and boundary integral solutions to three-dimensional spontaneous rupture, J. Geophys. Res., 110, B12307, doi:10.1029/2005JB003813.
Ely, G. P., S. M. Day, and J. B. Minster (2008). A support-operator method for viscoelastic wave modeling in 3D heterogeneous media, Geophys. J. Int. , 172, doi: 10.1111/j.1365-246X.2007.03633.x, 331-344.
Ely, G., S.M. Day, and J-B. Minster (2009). Dynamic rupture models for the southern San Andreas fault, *Bull. Seism. Soc. Am.*, *100* (1), 131-150, doi:10.1785/0120090187.
Ripperger, J., J. P. Ampuero, P.M. Mai, and D. Giardini (2007). Earthquake source characteristics from dynamic rupture with constrained stochastic fault stress, J. Geophys. Res. 112: B04311, doi:10.1029/2006JB004515.
Ripperger, J.; P. M. Mai and J.-P. Ampuero (2008) Variability of near-field ground motion from dynamic earthquake rupture simulations Bull. Seism. Soc. Am., 98 (3), 1207-1228; doi:10.1785/0120070076
Sibson, R.H. (1991). Loading of faults to failure, Bull. Seismol. Soc. Am., 81, 2493-2497.

Pseudo-dynamic Rupture Model Generator, SongRMG, Ver 1.0

Short summary

Author(s):	**S.G. Song**
Institution(s):	**ETH Zurich**

Code level:	Research
Language:	Matlab
Rupture description:	Pseudo-dynamic (Kinematic)
Green's function comp. method:	NA
Tested operating system:	Linux

Software objectives

This pseudo-dynamic rupture model generator (RMG) produces a number of rupture scenarios with a full description of spatio-temporal evolution of slip velocity function at each grid on the finite fault. The generated finite source models are to be used to simulate ground motions and to investigate the effect of earthquake source on near-source ground motion characteristics.

Methodology

Song et al. (2009) and Song & Sommerville (2010) originally introduced the main idea and mathematical framework in the rupture model generator, and they were expanded and improved by following studies (Song & Dalguer 2013; Song et al. 2013). A set of spatial random fields model the spatial distribution of several key kinematic source parameters, such as slip, rupture velocity, and peak slip velocity. In other words, one random variable is assigned to every subfault patch for each source parameter. If we have three source parameters, there are 3 random fields. The number of random variables for each random field is equal to the number of subfault patches on the finite fault. The random field model is constrained by rupture dynamics and past events in the framework of 1-point and 2-point statistics (Figure 10). 1-point statistics is a marginal probability density function at a given point on the fault. If we assume the Gaussian distribution, mean and standard deviation are the two main representative parameters. They control the possible range of values for each source parameter. For example, they control whether the rupture velocity is centered at a certain value with small variation, or has a wide range of variation with very low and high velocity, including supershear rupture. 2-point statistics is composed of both auto and cross-correlation. Autocorrelation controls the heterogeneity of each source parameters while cross-correlation controls coupling between source parameters. Figure 11 shows an example of auto- and cross-correlation structures extracted from a spontaneous dynamic rupture model.

Once we have targeted 1-point and 2-point statistics, we can generate a number of rupture scenarios by Monte Carlo sampling, assuming the multi-variate Gaussian distribution. We first construct a covariance matrix, given the target auto- and cross-correlation structures, and simulate the spatial distribution of source parameters that satisfy the target covariance matrix using the Cholesky factorization. Mean, standard deviation, and even the shape of marginal probability density function can be adjusted afterwards. Finally we combine the simulated spatial distribution of source parameters with a prescribed shape of slip velocity function, and produce a full description of finite source model. Song et al. (2013) provide the detailed description of the stochastic source modelling method.

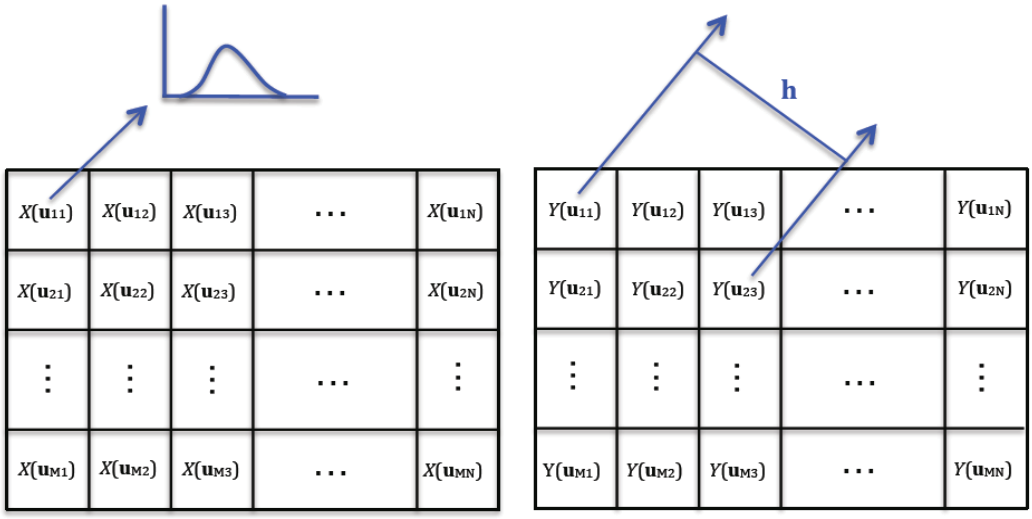

Figure 10. 2D distribution of random variables assigned to each source parameter on a planar fault, i.e., $X(\mathbf{u}_{ij})$ and $Y(\mathbf{u}_{ij})$ are random variables that represent one of source parameters such as slip, rupture velocity, slip velocity, and slip duration. $\mathbf{u}_{ij}$ is a location vector and **h** is a separation vector between two random variables. Random variables, *X* and *Y,* have their own uni-variate (1-point) probability density function (PDF) at a given subfault patch, and 2-point correlation structures can also be inferred as a function of **h** (Song & Dalguer 2013).

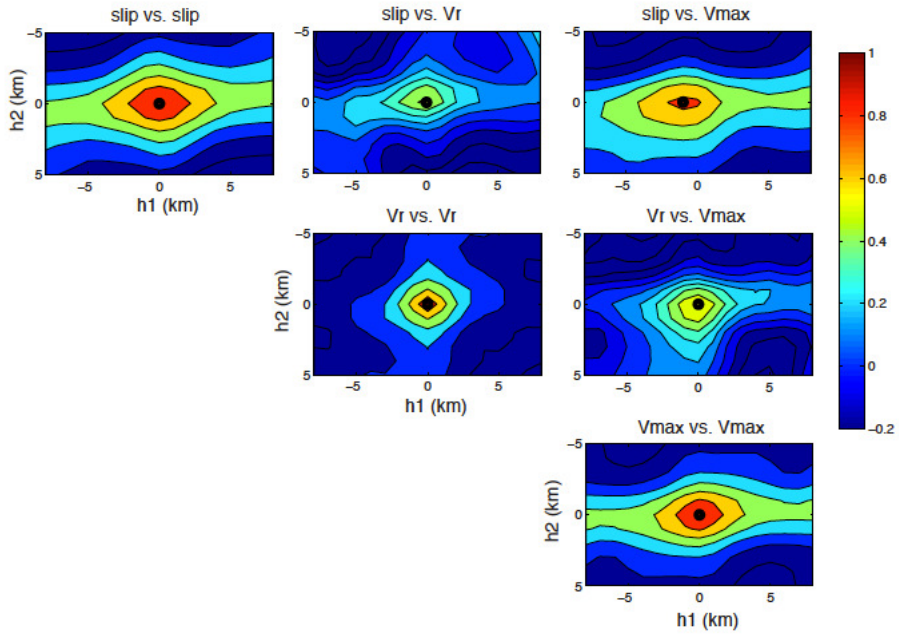

Figure 11. 2-point correlation structure extracted from a spontaneous dynamic rupture model. The diagonal blocks indicate the autocorrelation of each source parameter and the off-diagonal blocks indicate the cross-correlation between source parameters (Song et al. 2013).

Input

The RMG requires two input files. The first input file (left panel in Figure 12) describes the location, geometry, and dimension of a finite source. The second input file (right panel in Figure 12) defines target 1-point and 2-point statistics.

```
% Coded by Song, S. (April. 2013)
% Basic input parameters to describe a finite source model

function [rup] = gen_src(rup)

% Basic information for an event
rup.outfl = ['rup_' rup.name '.mat'];

rup.target_Mw   = 6.73;

rup.num = 50;         % number of simulation

rup.elon = -118.515;  % longitude, top center of the fault plane in degree
rup.elat =   34.344;  % latitude,  top center of the fault plane in degree

rup.L    = 20;        % fault length (along-strike) in km
rup.W    = 25;        % fault width (along-dip) in km

rup.stk  = 122;       % strike in deg.
rup.dip  = 40;        % dip in deg.
rup.rak  = 105;       % rake in deg.

rup.dtop = 5.;        % depth to top of fault
rup.shyp = 6.0;       % along strike location (from top center) of hypocenter
rup.dhyp = 19.4;      % along dip location (from top edge) of hypocenter

rup.dx   = 0.2;       % grid size (along-strike) in km
rup.dz   = 0.2;       % grid size (along-dip) in km

rup.svf.type = 'pliu';   % currently 'tri','rec','pliu', 'etinti' available
rup.svf.dt   = 0.1;
%%% End of inputs~~~~~~~~~~~~~~~~~~~~~~~~~~~~~~~~~~~~~~~~~~~~~~~~~~~~~~~~~~~~
```

```
%%% Coded by Song, S. (April. 2013)
%%% Set up target 1-point and 2-point statistics

function [rup] = gen_stats(rup)

%%%          [slip Vr Vmax risT];
rup.p1.min = [0   0.5 1.0 0.1];
rup.p1.max = [500 6.0 500 10];

rup.lambda = 1; % min wavelength = 10 km
rup.fN = 6;

rup.p2.tag = 'positive_eigen';

%%% 1-point and 2-point statistics of source parameters
% mod_vec = [slip Vr Vmax]
rup.p1.mu = [100 3.0 200];
rup.p1.sig = [50 0.1 50];

rup.p2.ax = [10 10 10;nan 10 10; nan nan 10];
rup.p2.az = [6 6 6; nan 6 6; nan nan 6];

rup.p2.cc = [1 0.6 0.6; nan 1 0.6; nan nan 1];

rup.p2.RDx = [0 0 0; nan 0 0; nan nan 0];
rup.p2.RDz = [0 0 0; nan 0 0; nan nan 0];
```

Figure 12. Two input files required running the rupture model generator (RMG).

Output

The RMG produces two output files. The first one (left panel in Figure 13) is a MATLAB data file that contains all relevant input, output, and control parameters in stochastic modelling. The second output file (right panel in Figure 13) is an ASCII file that contains information about the spatio- and temporal evolution of slip velocity function in the standard rupture format (SRF). The SRF is initially designed by R. Graves (USGS).

```
rup =

        name: 'Northridge'
       outfl: 'rup_Northridge.mat'
   target_Mw: 6.7300
         num: 50
        elon: -118.5150
        elat: 34.3440
           L: 20
           W: 25
         stk: 122
         dip: 40
         rak: 105
        dtop: 5
        shyp: 6
        dhyp: 19.4000
          dx: 0.2000
          dz: 0.2000
         svf: [1x1 struct]
          nx: 100
          nz: 125
          lx: [1x100 double]
          lz: [1x125 double]
         dis: [125x100 double]
          p1: [1x1 struct]
      lambda: 1
          fN: 6
          p2: [1x1 struct]
       eigen: [37500x1 single]
        slip: [1x1 struct]
          Vr: [1x1 struct]
         psv: [1x1 struct]
        risT: [1x1 struct]
          Mo: [1x50 single]
          Mw: [1x50 single]
        rupT: [1x1 struct]
        psv1: [1x1 struct]
```

```
1.0
PLANE 1
 -118.5150    34.3440     100     125     20.00     25.00
    122.00      40.00    5.00    6.00     19.40
POINTS   12500
  -118.6069    34.3906    5.06     122.00      40.00 4.000000e+08   15.30  0.1000
    105.00     101.79     54        0.00      0       0.00      0
5.109870e-07   1.007300e+01   2.622403e+01   4.557582e+01   6.432134e+01   7.860106e+01
8.540586e+01   8.370083e+01   7.497781e+01   6.141723e+01   4.631845e+01   3.334252e+01
2.561125e+01   2.411675e+01   2.361993e+01   2.306275e+01   2.244832e+01   2.178009e+01
2.106183e+01   2.029754e+01   1.949153e+01   1.864831e+01   1.777262e+01   1.686936e+01
1.594360e+01   1.500055e+01   1.404548e+01   1.308375e+01   1.212077e+01   1.116193e+01
1.021262e+01   9.278151e+00   8.363775e+00   7.474619e+00   6.615677e+00   5.791756e+00
5.007492e+00   4.267273e+00   3.575258e+00   2.935326e+00   2.351073e+00   1.825768e+00
1.362364e+00   9.634604e-01   6.312920e-01   3.677249e-01   1.742358e-01   5.191322e-02
1.440472e-03   0.000000e+00   0.000000e+00   0.000000e+00   0.000000e+00   0.000000e+00
  -118.6051    34.3896    5.06     122.00      40.00 4.000000e+08   15.69  0.1000
    105.00     105.29     43        0.00      0       0.00      0
6.784940e-07   1.876937e+01   4.918079e+01   8.195019e+01   1.062245e+02   1.137158e+02
1.038529e+02   8.184709e+01   5.640268e+01   3.753912e+01   3.212290e+01   3.127864e+01
3.030314e+01   2.920540e+01   2.799558e+01   2.668485e+01   2.528532e+01   2.380992e+01
2.227229e+01   2.068664e+01   1.906761e+01   1.743017e+01   1.578945e+01   1.416061e+01
1.255868e+01   1.099850e+01   9.494457e+00   8.060457e+00   6.709759e+00   5.454828e+00
4.307274e+00   3.277688e+00   2.375597e+00   1.609326e+00   9.859614e-01   5.112598e-01
1.896062e-01   2.397730e-02   0.000000e+00   0.000000e+00   0.000000e+00   0.000000e+00
0.000000e+00
```

Figure 13. Two output files. (a) MATLAB file, (b) ASCII file (Standard Rupture Format)

Performances

The code requires MATLAB with two additional toolboxes (‘mapping’ and ‘statistics’). The

computational cost is relatively cheap for small to moderate sized problems, i.e., coarse grid and small events (grid spacing >= 1 km or M < 6.5), but it may significantly increase for large problems (grid spacing < 0.2 km and M > 6.5). For a testing problem (grid spacing = 0.2 km, M = 6.7), it requires about 12-hour wall clock computing time and 32 GByte memories. We have a plan to reduce the computational cost by applying more efficient algorithms in the future development. In addition, most computational costs are driven by the Cholesky and eigenvalue decomposition, which are needed once for a given correlation structure. This means that for the same target correlation structure we perform the matrix decomposition just one time, and generate a number of rupture scenarios without additional costly matrix decomposition procedures even with a current version of the code.

Example

Figures 14 and 15 show two examples of pseudo-dynamic source modelling. In Figure 14, earthquake slip is fixed, and we simulate two temporal source parameters, both rupture velocity and peak slip velocity, given the target 1-point and 2-point statistics. Since the earthquake slip is fixed, simulated temporal source parameters are derived from the probability density function conditioned on the fixed slip, thus they show less variability between models. Figure 15 shows three difference source models for the 1994 Northridge, California, event. Since the earthquake slip is not fixed here, we can see more variability among simulated source models.

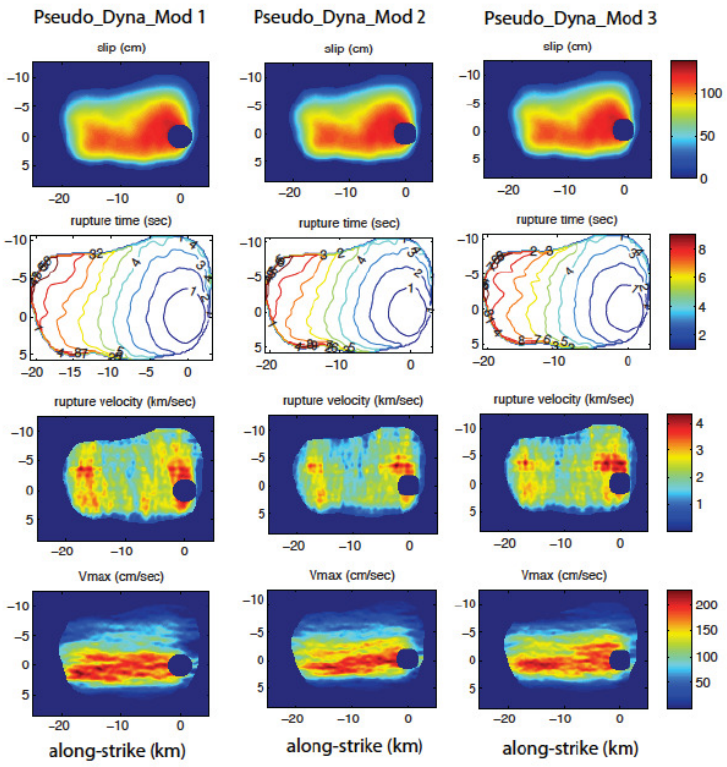

Figure 14. Pseudo-dynamic source models generated by stochastic modelling (Song et al., 2013). In this case, earthquake slip is fixed and temporal source parameters are simulated, given the slip, and the target 1-point and 2-point statistics.

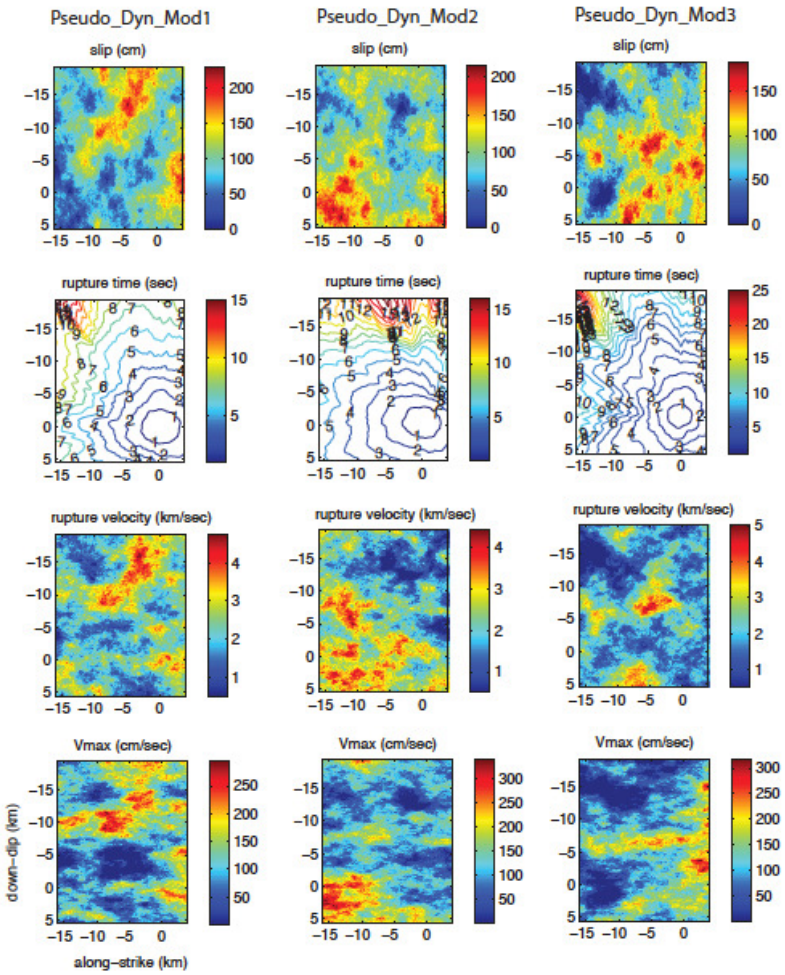

Figure 15. Pseudo-dynamic source models designed for the 1994 Northridge, California, event. The rupture dimension and hypocentre location are fixed by the Northridge event, but the spatial distribution of source parameters are generated by stochastic modelling.

Related publications

S. Song, L.A. Dalguer, and P.M. Mai (2013). Pseudo-dynamic source modeling with 1-point and 2-point statistics of earthquake source parameters, *Geophys. J. Int.*, in revision.

S. Song, and L.A. Dalguer (2013). Importance of 1-point statistics in earthquake source modeling for ground motion simulation, *Geophys. J. Int.*, 192, 1,255-1,270.

S. Song, P. Somerville (2010). Physics-based earthquake source characterization and modeling with Geostatistics, *Bull. Seism. Soc. Am.* 100, 482-496.

S. Song, A. Pitarka, and P. Somerville (2009). Exploring spatial coherence between earthquake source parameters, *Bull. Seism. Soc. Am.* 99, 2,564-2,571.

Software availability

Potential users can contact S.G. Song (ETH Zurich, song@sed.ethz.ch) for the code. We plan to make it public in near future.